

TITLE: CHK1 inhibition synergizes with gemcitabine initially by destabilizing the DNA replication apparatus

AUTHORS AND AFFILIATIONS:

Siang-Boon Koh¹, Aurélie Courtin^{1,3}, Richard J. Boyce², Robert G. Boyle², Frances M. Richards¹ and Duncan I. Jodrell¹

¹Cancer Research UK Cambridge Institute, University of Cambridge, Cambridge, CB2 0RE, UK

²Sentinel Oncology Limited, Cambridge, CB4 0EY, UK

³Current address: Astex Pharmaceuticals, Cambridge, CB4 0QA, UK

RUNNING TITLE:

Mechanistic insights on CHK1 inhibition

KEYWORDS:

CHK1; gemcitabine; synergy; cell cycle checkpoint; DNA damage response

FINANCIAL SUPPORT:

This study was funded by Cancer Research UK via Institute Senior Group Leader funding (C14303/A17197) to DI Jodrell, and by Sentinel Oncology through an award from Innovate UK.

CORRESPONDING AUTHOR:

Frances M. Richards

CRUK Cambridge Institute, Li Ka Shing Centre, Box 278, Robinson Way, Cambridge, CB2 0RE, UK

Telephone: +44(0)1223769633

Email: Fran.Richards@cruk.cam.ac.uk

POTENTIAL CONFLICTS OF INTEREST:

RG Boyle is a founder of Sentinel Oncology. RJ Boyce is an employee and shareholder of Sentinel Oncology. DI Jodrell was in receipt of a grant from Sentinel Oncology to support laboratory studies with S1181. SB Koh, A Courtin and FM Richards disclose no potential conflicts of interest.

TEXT: 4628 words (excluding references and figure legends)

ABSTRACT

Combining cell cycle checkpoint kinase inhibitors with the DNA-damaging chemotherapeutic agent gemcitabine offers clinical appeal, with a mechanistic rationale based chiefly on abrogation of gemcitabine-induced G2/M checkpoint activation. However, evidence supporting this mechanistic rationale from chemosensitization studies has not been consistent. Here we report a systematic definition of how pancreatic cancer cells harboring mutant p53 respond to this combination therapy, by combining mathematical models with large-scale quantitative biological analyses of single cells and cell populations. Notably, we uncovered a dynamic range of mechanistic effects at different ratios of gemcitabine and CHK1 inhibitors. Remarkably, effective synergy was attained even where cells exhibited an apparently functional G2/M surveillance mechanism, as exemplified by a lack of both overt premature CDK1 activation and S-phase mitotic entry. Consistent with these findings, S/G2 duration was extended in treated cells, leading to an definable set of lineage-dependent catastrophic fates. At synergistic drug concentrations, global replication stress was a distinct indicator of chemosensitization as characterized molecularly by an accumulation of S-phase cells with high levels of hyperphosphorylated, RPA-loaded single-stranded DNA. In a fraction of these cells, persistent genomic damage was observed, including chromosomal fragmentation with a loss of centromeric regions that prevented proper kinetochore-microtubule attachment. Together, our results suggested a "foot-in-the-door" mechanism for drug synergy where cells were destroyed not by frank G2/M phase abrogation, but rather by initiating a cumulative genotoxicity that deregulated DNA synthesis.

INTRODUCTION

The DNA damage response (DDR) to a vast majority of genomic insults is orchestrated by the activation of two key phosphatidylinositol 3-kinase-related kinases, ATM and ATR. Upon recruitment to damage sites, ATM and ATR phosphorylate a number of substrates, including checkpoint kinase CHK1 (CHEK1), which in turn mediate cell cycle arrest to facilitate DNA repair (1). An intact ATM/ATR-CHK1 signaling cascade is integral to genomic integrity and therefore survival. Because cancer cells frequently harbor surveillance defects, they are reliant on the residual functional processes of the DDR machinery (2). Inhibition of the DDR with checkpoint kinase inhibitors thus heralds a promising cancer therapeutic strategy for chemosensitization.

Early prototypes of non-selective checkpoint kinase inhibitors caffeine and UCN-01 have been shown to induce unscheduled mitosis following abrogation of DDR-induced cell cycle arrest (3,4). This has subsequently inspired an accumulating body of evidence associating CHK1 inhibition with G2/M checkpoint abrogation, characterized by premature chromosomal condensation, inflated mitotic index and aberrant chromosomal structures (5-7). Against this background, ongoing clinical trials of CHK1 inhibitors with DNA-damaging agents are chiefly based on the notion of G2/M checkpoint abrogation (8). Nonetheless, owing to the multiple roles of CHK1 in cell cycle regulations, it is not definitive if this represents the predominant mechanism of chemosensitization (9).

Among all chemotherapy agents, the greatest potentiation by CHK1 inhibitors has been reported with antimetabolites, notably gemcitabine (10). Gemcitabine is standard for patients with pancreatic ductal adenocarcinoma, one of the most intractable of human malignancies (11). Here, we took a systematic approach to

elucidate how pancreatic tumor cells responded to gemcitabine and CHK1 inhibition. Using mathematical models coupled with cytotoxicity assays, we first identified concentration ratios of gemcitabine and CHK1 inhibitors that induced synergistic growth inhibition. We then employed population- and single-cell-based assays to quantitatively define cell cycle modulation and cell behaviors. Our study reveals a level of mechanistic complexity that offers conceptually important insights into the dynamic interplay between gemcitabine and CHK1 inhibition.

MATERIALS AND METHODS

Cell culture and chemicals

Human pancreatic cancer cells (MIA PaCa-2, Panc-1), colorectal cancer cells (HT-29) and non-malignant lung fibroblast (IMR-90) were obtained from either the European Collection of Cell Cultures or the American Type Culture Collection. They were authenticated using either Promega GenePrint10 system or Promega PowerPlex 16HS kit, and were grown in DMEM with 10% FBS (GIBCO). Murine pancreatic cancer cells K8484 were established from a KRas^{G12D}; p53^{R172H}; Pdx1-Cre mouse (12) and were grown in DMEM with 5% FBS. All cell lines were grown up to a maximum of 20 passages and for fewer than 6 months following resuscitation. They were routinely verified to be mycoplasma-free using the Mycoprobe Mycoplasma Detection Kit (R&D Systems). Gemcitabine (Tocris), S1181 (Sentinel Oncology; patent application: WO/2011/ 141716, compound Example 20), CHIR-124 (Selleck Chemicals), roscovitine (Sigma-Aldrich), Cdc7i (PHA767491, Tocris) and CDK1i (RO3306, Calbiochem) were dissolved in DMSO in aliquots of 10-30mM, kept at -20 degree Celsius and used within 3 months. Final DMSO concentrations ($\leq 0.2\%$) were kept constant in all experiments.

Cell cycle synchronization and flow cytometry

For G1/S synchronization, thymidine (Sigma-Aldrich) was dissolved in sterile PBS and used at a final concentration of 2mM following a 16-hour block/8-hour release/16-hour block protocol. For G2/M synchronization, CDK1i (RO3306, Calbiochem) was dissolved in DMSO and used at a final concentration of 9uM for 20 hours. To analyze cell cycle distributions, cells were trypsinized, fixed with either 70% ethanol or 4% paraformaldehyde, stained with antibodies and counterstained with propidium iodide. Samples were analyzed on the BD FACSCalibur flow

cytometer (BD Biosciences). ≥ 10000 events were collected per sample, and data were processed using the FlowJo software.

Clonogenic assay

Cells were plated 24 hours prior to treatment. Following treatment, equal numbers of viable cells from each sample were reseeded in fresh medium and left to grow.

Seven days later, cells were fixed with 70% methanol and stained with 5% Giemsa (Sigma-Aldrich). Colonies were imaged and quantified using the ImageQuant TL software (GE Healthcare). Plating efficiency was calculated from the ratio of the number of colonies to the number of cells seeded. The number of colonies that arose after treatment was expressed as surviving fraction. This was derived from the ratio of the number of colonies formed after treatment to the number of cells seeded multiplied by plating efficiency of the control.

Immunostaining and immunoblotting

For immunostaining, cells were fixed with 4% paraformaldehyde, permeabilized with 0.3% Triton X-100, stained with antibodies and counterstained with DAPI. To visualize centromeres and kinetochores, 100% methanol fixation method was used. EdU and TUNEL Click-it assays were performed on paraformaldehyde-fixed samples based on Click-it reaction according to manufacturer's instructions (Life Technologies). For immunoblotting, whole-cell extracts were obtained by lysis in RIPA buffer (50mM Tris pH8.0, 2mM EDTA, 150mM sodium chloride, 1% NP-40, 0.5% sodium deoxycholate, 0.1% SDS) and resolved using the SDS-PAGE gel system (Life Technologies). Blots were analyzed using the Odyssey Infrared Imaging System (LI-COR).

IncuCyte time-lapse imaging

Images were acquired with the IncuCyte Live Cell Imaging microscopy (Essen Bioscience) at every three hours under cell culture conditions with 10X objective. Averaged cell confluence was calculated from three random fields of view per well using the IncuCyte in-built algorithm. Relative confluence values were obtained by normalizing each value to the time zero value in each sample.

Metaphase spreads

Cells were treated with 0.1ug/mL colcemid for 45 minutes, trypsinized and treated in a drop-wise manner with pre-warmed 0.075M KCl. After 15-minute incubation at 37°C, cells were sequentially fixed in freshly prepared methanol:acetic acid mix (3:1 then 3:2). After an overnight incubation at -20°C, cells were dropped onto coverslips and stained with ProLong® Gold Antifade Mountant with DAPI (Life Technologies).

Statistical analyses

Data were analyzed using the GraphPad Prism built-in tests. For comparison among three or more groups, an ordinary one-way ANOVA analysis followed by post hoc tests was performed. The following asterisk rating system for p-value was used:

* $p \leq 0.05$, ** $p \leq 0.01$, *** $p \leq 0.001$, **** $p \leq 0.0001$.

Supplementary Materials and Methods include antibodies; cytotoxicity agent combination assay and synergy calculation; acquisition, processing and analysis of live-cell time-lapse sequences; and quantitative fluorescence-based microscopy.

RESULTS

Mathematical modelling identifies effective synergy between gemcitabine and CHK1i at sub-GI₅₀ concentrations

A drug discovery program identified S1181 as a novel selective small molecule inhibitor of CHK1 (IC₅₀=2.5nM) (Fig. 1A, Supplementary Fig. S1A, Table S1). Using S1181 as a CHK1i tool compound, we performed sulforhodamine B cytotoxicity assays to test its effects with gemcitabine on human cancer cell lines (MIA PaCa-2, Panc-1, HT-29) and a mouse pancreatic cancer cell line, K8484, obtained from a KRas^{G12D}; p53^{R172H}; Pdx1-Cre mouse. To objectively identify the presence and region of synergy, we assessed each combination assay independently with three established mathematical models, i.e. Bliss, Loewe and Highest Single Agent models (see Supplementary Materials and Methods). To further the stringency of our criteria, we defined “effective synergy” as the minimum concentrations that produced >90% growth inhibition. Consistently, effective synergy was found at sub-GI₅₀ concentrations in all tumor cell lines but not in non-malignant IMR-90 cells (Fig. 1B, Supplementary Fig. S1B).

Target inhibition occurred at synergistic concentrations, as demonstrated by attenuation of CHK1 autophosphorylation at S296 and phosphorylation of ATR targets CHK1 S317 and CHK1 S345 (Fig. 1C, Supplementary Fig. S1C) (13). With 24 hours of combination treatment, ATM S1981 nuclear foci were observed, alongside the upregulation of its downstream substrates CHK2 T68 and H2AX S139 (γH2AX), implying elevated DNA damage that involved fork breakage (Fig. 1C-D). With 72 hours of combination treatment, cell viability was severely affected, as evidenced by increase in γH2AX, cleaved PARP and caspase-3, apoptotic bodies, and TUNEL staining (Supplementary Fig. S1D-F). Long-term clonogenic assays

corroborated a durable synergistic relationship between the two agents (Fig. 1E, Supplementary Fig. S1G). Together, the data demonstrate that sub-GI₅₀ concentrations of gemcitabine and CHK1i are sufficient to yield synergistic growth inhibition.

Forced mitotic entry is not a common determinant of effective synergy

A widely held assumption is that CHK1 inhibition abrogates the G2/M checkpoint by triggering inappropriate CDK activation, leading to forced mitotic entry. To test this notion in the context of effective synergy, we interrogated CDK activation status (Fig. 2A). Unexpectedly, we found no apparent disinhibition of CDK activity (i.e. no decrease in the inactive form CDK Y15) upon gemcitabine+CHK1i treatment at synergistic concentrations. To rule out potential off-target effects of S1181, we used another structurally distinct potent CHK1-specific inhibitor CHIR-124 and achieved similar outcomes at relevant synergistic concentrations (Supplementary Fig. S2A-B). We investigated if these molecular changes were accompanied by forced mitosis. Both quantitative immunoblotting and cytometry for mitotic marker HH3 S10 (pHH3) confirmed that the synergistic combination did not substantially elevate the mitotic population compared to single-agent controls (Fig. 2A, Supplementary Fig. S2C). Furthermore, DNA content of the mitotic cells treated with the synergistic concentrations was near 4N regardless of treatment duration (24-72 hours), suggesting an absence of forced S-phase mitotic entry (Fig. 2B and Supplementary Fig. S2D; see data for 10nM gemcitabine+1uM S1181).

Cancer cells display divergent mechanistic interpretations at different concentration ratios

A potential caveat of the above findings is that they were attained under fixed-ratio of gemcitabine and CHK1i, and thus did not capture the dynamic range within which

synergy may arise. To address this, we revisited the synergy plots and paired up a fixed concentration of CHK1i with low and high gemcitabine (Fig. 2C, Supplementary Fig. S2E). CHK1i with low gemcitabine, while synergistic, neither triggered CDK inactivation nor substantially altered the percentage of pHH3-positive population compared to single-agent control (Fig. 2C, compare lane 3 with lane 5). Conversely, with high gemcitabine, there was obvious G2/M checkpoint override exemplified by decreased CDK Y15 and elevated pHH3 (Fig. 2C, compare lane 4 with lane 6). Quantification of DNA content shows that, independent of treatment duration, pHH3-positive cells in high gemcitabine were consistently <3N, a signature of premature S-phase mitotic entry (Fig. 2B, Supplementary Fig. S2D; see data for 100nM gemcitabine+1uM S1181).

We did a reverse set of experiments, where a fixed gemcitabine was coupled with increasing CHK1i (Fig. 2D, Supplementary Fig. S2F). With low synergistic CHK1i, we did not see gross G2/M checkpoint abrogation as there was little change in the levels of CDK Y15 and pHH3. With higher CHK1i, CDK activation (reduced CDK Y15) that promoted mitotic entry (elevated pHH3) became more apparent. All these experiments were reproducible in cell lines with different synergistic concentrations (Fig. 2C-D, Supplementary Fig. S2E-F). To further verify these findings in the same setting, we employed yet another cell line HT-29, which has previously been shown to undergo unscheduled mitotic entry with CHK1 inhibition (14), and reached the same conclusions (Fig. 2E): with low synergistic gemcitabine (30nM) and CHK1i (1uM), the percentage of mitotic cells was not considerably different from single-agent controls and they had ~4N DNA content; with high gemcitabine (300nM) and CHK1i (5uM), there was an increase in <4N mitotic cells. Collectively, while our data are in line with previous reports on G2/M checkpoint abrogation at relatively high

concentrations of gemcitabine or CHK1i, they argue for the hitherto discounted possibility that this is dispensable at optimal synergistic ratios of gemcitabine and CHK1i.

Delayed S progression is a denominator of cytotoxicity, regardless of the mode of elimination

The foregoing experiments suggest that forced mitotic entry is inadequate to explain the effective synergy between gemcitabine and CHK1i. First, the principle of effective checkpoint abrogation would apply if cells experience supra-physiological levels of DNA damage in the first instance; such was not the case with sub-GI₅₀ gemcitabine alone (Fig. 1, Fig. 2). Second, cells treated with gemcitabine at synergistic concentrations in the absence of CHK1i remained cycling for at least 72 hours, incongruent with the notion of an alarmed G2/M checkpoint (Supplementary Fig. S3A). Third, given the nominal extent of checkpoint activation, checkpoint abrogation by CHK1i would be more a conditional than an absolute requirement for synergy, explaining the absence of overt perturbation on CDK1 activity (Fig. 2).

To validate these conclusions, we reasoned that there must be a mechanistic underpinning that preceded G2/M checkpoint abrogation. We performed quantitative flow cytometry to determine cell cycle profiles. Consistently, gemcitabine+CHK1i at synergistic concentrations resulted in an increase in S-phase population (Fig. 3A, Supplementary S3B, Table S2). To directly correlate spatiotemporal configuration of cell-cycle dynamic with treatment conditions, we harnessed the Fluorescent Ubiquitination-based Cell Cycle Indicator (Fucci) technology, which distinguished S/G2-M cells from G1 cells based on fluorescently tagged forms of geminin (green) and Cdt1 (red), respectively (Supplementary Fig. S3C) (15). In tandem, we developed a live-cell tracking methodology that allowed measurement of S/G2

duration in an automated and reproducible fashion (see Supplementary Materials and Methods). Analyzing over 2000 single cells, we found that the averaged S/G2 duration in gemcitabine-treated cells ($10.4 \pm 0.25\text{h}$) was 2 hours longer than control ($8.6 \pm 0.16\text{h}$) and CHK1i ($8.2 \pm 0.16\text{h}$) (Fig. 3B). Gemcitabine+CHK1i prolonged the interphase residence time by another 3 hours ($13.3 \pm 0.53\text{h}$), consistent with the accumulation of the S-phase population (Fig. 3A).

Time-lapse analysis showed diverse cell fates following gemcitabine+CHK1i (Fig. 3C). To facilitate comparative analyses without compromising the complexity, the first-generation fate profile of each individual cell from the time of treatment to the end of first mitosis (if occurred) was plotted (Fig. 3D). Of the 115 asynchronous cells, eighty-three cells proceeded to the next cell cycle while thirty-two cells experienced adverse fate in the first observed cell cycle. Among these thirty-two cells, two died in mitosis, fifteen failed cytokinesis, while the remaining fifteen experienced prolonged arrest (three), senescence (seven) or death (five) in S/G2 interphase without ever entering mitosis. Notably, twenty-three out of twenty-nine cells in the fourth quartile of S/G2 duration experienced adverse fates. All these data stood in contrast to the first-generation fate profiles of the control, where all the 100 cells entered mitosis following a relatively short S/G2 duration and successfully underwent cytokinesis (Supplementary Fig. S3D). Together, these data support a model where, irrespective of how a cell is eliminated, prolonged S duration appears to be a key that presages an unfavorable biological event.

Cell fate is influenced by the extent of agent exposure across generations

If the above hypothesis is generally applicable, we postulated that there should be a lineage-dependent phenomenon where cell fate could be extrapolated from the initial state of a cell. To test this, we first performed a pedigree examination

(Supplementary Fig. S3E). We tracked cells that underwent one mitotic division in order to identify daughter cells derived from the same mother. We then determined the fate of 75 pairs of sisters. We found that most sisters shared the same fate upon gemcitabine+CHK1i. Based on this and our earlier results, we reasoned that cell fate decision could be dependent on the degree of maternal exposure during S/G2. Strikingly, we found that offspring of mothers with protracted S/G2 progression were more prone to some form of adverse fate (failed cytokinesis, interphase arrest, senescence, death) than those with mothers of shorter S/G2 duration (Fig. 3E). Furthermore, linearity between the S/G2 duration and mitotic duration implies a causal connection between the interphase state and subsequent mitotic state, providing an explanation to previous work that implicates CHK1i in activating the spindle assembly checkpoint (16).

Next, we asked if S/G2 duration progressively lengthened through generations. To address this in a manner that ensured complete retrieval of temporal data, we focused on cells that were in G1 phase at the start of each experiment and that had at least one dividing daughter. Significantly, S/G2 duration doubled over two generations (Fig. 3F). This was accompanied by a five-fold increase in mitotic duration (Supplementary Fig. 3SF). Furthermore, virtually all second-generation cells affected by the temporal inflation failed to divide, consistent with the phenomenon seen in the first-generation population. As a unifying validation to all our findings, we determined the S/G2 and mitotic durations of cells that proceeded into the second cell cycle in order to correlate them to their fate. Whereas 72% (83 out of 115 cells) underwent division in the first cell cycle, the percentage dropped to 15% (25 out of 164 cells) in the second round (Supplementary Fig. S3G). Moreover, in daughters that attempted a second mitosis, we again saw a positive association between the

length of S/G2 and mitosis, with those cells at the higher ends being more vulnerable to cytokinesis failure (Supplementary Fig. 3SH). Together, our lineage-tracing analyses highlight the effects of agent exposure during interphase and how that could propagate across the descendants of an insulted cell.

CHK1 inhibition triggers global replication stress by deregulating the replication checkpoint

The distinctive phenotype of perturbed S progression prompted us to interrogate the intra-S replication activity upon treatment. First, we synchronized MIA PaCa-2 cells at the G1/S border and released them into treatment conditions, labelling with EdU over 1-4 hours (Fig. 4A). To enumerate the fraction of replicating cells, we employed quantitative fluorescence-based microscopy, which enabled the analysis of thousands of single-cell measurements based on multiple parameters of the fluorescent readout (see Supplementary Materials and Methods). We found that CHK1i caused a more rapid initial uptake of EdU in MIA PaCa-2 cells compared to control or gemcitabine 2-3 hours following release. When asynchronous populations of another cell line HT-29 were treated with CHK1i and then labelled with a shorter pulse of EdU, we again observed a significant increase in replicating cells (Supplementary Fig. S4A). Collectively, the data suggest enforced initiation and promotion of DNA synthesis with CHK1 inhibition.

Forced DNA synthesis is a source of replication stress (17). In response to replication stress, single-stranded DNA (ssDNA)-coating trimeric RPA protein is recruited and phosphorylated at multiple sites, with RPA32 S4/8 being found in the most hyper-phosphorylated form of the protein (18). We observed an increase in phosphorylated RPA upon gemcitabine+CHK1i treatment but not with either agent alone (Supplementary Fig. S4B). This exclusivity highlights the dependency between

the two agents in deregulating the replication program. Furthermore, quantitative microscopy reveals that cells with the highest degree of RPA32 S4/8 were also experiencing substantial fork breakage, as evidenced by co-staining with γ H2AX (Fig. 4B, Supplementary Fig. S4C). The majority of these cells were in S-phase (Supplementary Fig. S4D). High-resolution confocal imaging shows nucleus-wide staining of activated RPA in these cells, indicative of long stretches of ssDNAs with stalled replication forks (Supplementary Fig. S4E). On the other hand, γ H2AX was found in heterochromatic regions, consistent with the presence of replication intermediates refractory to repair (19). Together, the data suggest that gemcitabine+CHK1i overloads the replication machinery through improper initiation and promotion of DNA synthesis, eventually leading to the pathological outcome of unresolved DNA lesions.

A reverse prediction was that suppression of DNA synthesis should relieve global replication stress. To this end, we exploited the paradigm that CHK1 regulates origin activity and that origin activity requires CDK2 (20). We found that application of a broad CDK inhibitor roscovitine with gemcitabine+CHK1i reversed S-phase accumulation within 12 hours (Fig. 4C). By 24 hours, roscovitine markedly subdued γ H2AX and RPA32 S4/8 expressions in treated cells, indicating mitigation of replication stress (Fig. 4D). These results were reproduced by inhibiting Cdc7, another regulator of origin firing (Fig. 4C-D).

Given that inhibition of CDKs and Cdc7 is cytostatic, a counter-argument would be that the apparent rescue was an indirect effect of reduced genome incorporation of gemcitabine. To address this, we asked whether restraining DNA replication in gemcitabine+CHK1i could abolish the synergistic growth inhibition. We performed long-term proliferation studies (Fig. 4E, Supplementary Fig. S4F). Significantly, cell

proliferation was restored to control levels by roscovitine and Cdc7i, partially or fully so depending on cell lines. Substituting roscovitine with a specific CDK1i at sub-arresting concentrations did not redress growth retardation by gemcitabine+CHK1i (Supplementary Fig. S4G). Together, these data show that, at sub-G₁₅₀ concentrations, CHK1i synergizes with gemcitabine mainly by perturbing the S-phase homeostasis through deregulated DNA replication, not by G2/M checkpoint abrogation.

Mitotic aberrance is a consequence of deranged replication machinery

Emerging evidence suggests that genomic insults in interphase can persist into mitosis (21). Given that a fraction of cells underwent prolonged mitosis upon gemcitabine+CHK1i, we proceeded to determine the nuclear morphology of these cells. Aberrant mitotic architectures were significantly found in the combination treatment (Fig. 5A-B). These included misaligned metaphases, lagging chromosomes and anaphase bridges. When cells were synchronized at the G2/M border and released into gemcitabine+CHK1i, there was no evidence of gross mitotic aberrance (Supplementary Fig. S5A). This ruled out the possibility that CHK1 mitotic role was compromised (22). Together, the data suggest that preceding replication mishap is responsible for the aberrant mitotic manifestations.

We noticed that misaligned metaphases with dramatic dispersion of chromosomes were particularly common with CHK1 inhibition. Previous studies have invariably attributed this feature to checkpoint bypass, but have variously described it as disorganized spindle (23), centromere fragmentation (24) and failure of chromosomes with intact centromeres to align along the metaphase plate (14). To clarify, we stained cells for tubulin and found apparently normal bipolar microtubule organization (Fig. 5A). With z-stack confocal analysis, we found core component of

kinetochore outer plate HEC1 co-localizing exclusively with chromosomes at the metaphase plate (Fig. 5C). This was accompanied by the presence of genome material separate from the plate, indicative of acentric chromosomes. Similar spatial configuration was also observed with centromere DNA-binding CENP-B. Given that (peri)centromeric structures arise from heterochromatin, damage in this region would conceivably result in their defective formation. This is consistent with the observation that only with CHK1 inhibition (with or without gemcitabine) did γ H2AX propagate into heterochromatin (Supplementary Fig. S5B).

An alternative but not mutually exclusive explanation was chromosomal fragmentation, a phenomenon increasingly recognized as a form of mitotic death but often confused with premature chromosomal condensation (PCC) (25). To formally investigate this possibility, we performed immunofluorescence and found that (1) γ H2AX decorated aberrant mitoses, more so in those with severely tattered chromosomes (Fig. 5D), (2) mitoses were EdU-negative and were not actively replicating (Fig. 5E), and (3) mitotic aberrance was not abolished by CDK inhibitor co-treatment (Supplementary Fig. S5C). Furthermore, independent of combination treatment duration (24-72 hours), metaphase spreads showed various stages of chromosomal breakage demonstrated by differential cut sizes, suggesting that it was a cumulative process that occurred at single-cell level (Fig. 5F). Together, these data confirm chromosomal fragmentation, preclude PCC (26) and premise that the replication crisis invoked by gemcitabine+CHK1i could progressively culminate in mitotic disaster.

DISCUSSION

An overwhelming body of literature proposes that checkpoint abrogation by CHK1i in gemcitabine-treated cells drives them into premature mitosis. However, such abrogation has never been formally established as the cause of chemosensitization (9). Importantly, G2/M checkpoint bypass by CHK1i does not always correlate with gemcitabine sensitization (7). Our findings explain some of these apparent discrepancies.

We have demonstrated that the mechanistic properties of effective synergy between gemcitabine and CHK1i are in fact consistent but contingent on the degree of genotoxicity induced. This in turn is concentration-sensitive. The salient features of this modulation are generalized in Fig. 6A. By itself, low yet synergistic concentrations of gemcitabine retard DNA synthesis but do not elicit permanent proliferation blockade. Thus, delayed but timely mitotic CDK1 activation enables cells to cycle into mitosis. This places a limit on the extent of CDK1 disinhibition and hence checkpoint abrogation when CHK1 is inhibited. Counterintuitively, at higher gemcitabine concentrations (which by themselves are cytotoxic), the same extent of CHK1 inhibition triggers unscheduled CDK1 activation and premature S-phase mitosis. One scenario explaining this phenomenon is the synchronizing effects of high-concentration gemcitabine. At high concentrations, cells are uniformly and often irreversibly blocked in S-phase. Addition of CHK1i hence promotes simultaneous premature mitosis of these arrested cells, leading to an apparent inflation in CDK1 activity and mitotic index with $<4N$ state. Virtually all functional studies on CHK1i to date that have reported such phenomena base their conclusions on the higher end ($>GI_{50}$) of gemcitabine concentrations, as much as 10-200 times above the concentrations where effective synergy is typically observed (7,14,27-29).

We have shown that the immediate response of cells upon addition of CHK1i to gemcitabine at lower, synergistic concentrations is not premature S-phase mitotic entry. Instead, cells experience prolonged interphase with enhanced DNA damage and replication stress, reminiscent of the nucleus-wide replication catastrophe when ATR signaling is perturbed (30). A fraction of these cells enter mitosis, often with disastrous consequences. While this in principle suggests G2 abrogation, given the global mitotic CDK1 suppression and substantial delay in mitotic entry as well as the low concentrations of the agents used, the data are also compatible with the notion of G2 checkpoint adaptation. It has been shown that G2 adaptation can occur in human cells and is possible following pharmacological concentrations of genotoxic agents (31,32). Taken together, as opposed to blatant checkpoint abrogation, our study illustrates a “foot-in-the-door” phenomenon (Fig. 6B). This model proposes that premature S-phase mitotic entry is not the predominant route to chemosensitization. Instead, CHK1i synergizes with gemcitabine via a more subtle and far-reaching mechanism, i.e. first by engaging cells in disorderly replication, then committing them to elimination processes that could take place in and beyond mitosis.

Our mechanistic study raises several key issues regarding the development of CHK1i as cancer therapeutics. First, largely based on preclinical studies that have used high concentrations of genotoxic agents, emerging consensus on treatment regimen advocates a delayed administration of CHK1i (10,33). ~~However, early clinical results from UCN-01 trials suggest that delayed administration of the checkpoint kinase inhibitor has been suboptimal in chemosensitization, with inconsistent evidence of checkpoint bypass.~~ However, it is uncertain if any of the enhanced effect seen with a staggered regimen represents true synergy or if it is a result of accelerated (but not necessarily synergistic) cytotoxicity. In the most

promising clinical trial so far, two patients with pancreatic adenocarcinoma exhibited stable disease lasting > 10 months, and there was a partial response in a cholangiocarcinoma patient, in a Phase I dose escalation study, when CHK1i MK-8776 was given only 30 minutes after gemcitabine (34). We have shown with the aid of mathematical models that non-cytotoxic concentrations of gemcitabine and CHK1i could yield effective synergy in tumor cells when given together. We propose that simultaneous administration of both agents warrants further investigation. This is especially germane in view of the variable intratumoral gemcitabine levels expected in patients, owing to short half-life and poor drug delivery (12). Second, dose-dependent toxicities are a major cause of drug attrition. Clinical development of several checkpoint kinase inhibitors has been discontinued, the most recent being AZD7762 given its untoward cardiotoxicity (35). We have shown that a threshold of CHK1 inhibition beyond that necessary for synergy is required for overt checkpoint abrogation. As our data suggest that inhibition of S-phase activities of CHK1 is more relevant to chemosensitization, concurrent administration of gemcitabine and CHK1i would in principle obviate the need for G2/M checkpoint abrogation. We anticipate that metronomic gemcitabine, where low doses are given at frequent intervals, represents an opportunity where the synergistic interaction between the antimetabolite and CHK1i could be exploited (36). Third, low doses of gemcitabine and CHK1i would permit the possibility of triple drug therapies. This is potentially applicable to treatment modalities to which S-phase cells are particularly vulnerable, for example radiotherapy. In support of this and the notion that G2/M bypass is dispensable for synergy, radiosensitization has been reported to occur most optimally when CHK1 is inhibited during S-phase, but not when G2/M abrogation is maximal (37). Attractive concepts on chemoradiosensitization with checkpoint kinase

inhibitors have been proposed but remain largely unexplored (10). Our data illustrate a distinct mechanistic perspective on CHK1 inhibition that serves as a reference for future combination and scheduling work.

ACKNOWLEDGEMENTS

We thank Steve Jackson for critical reading of the manuscript; Fanni Gergely, Masashi Narita and Paul Edwards for insightful discussion; Scott Lyons and Esther Rodriguez for the Fucci cell line; Patrice Mascalchi for microscopy expertise; and members of the Pharmacology & Drug Development Group as well as CRUK Cambridge Institute core facilities for technical support. This work was funded by Cancer Research UK (C14303/A17197) and by Sentinel Oncology through an award from Innovate UK.

REFERENCES

1. Jackson SP, Bartek J. The DNA-damage response in human biology and disease. *Nature* 2009;461(7267):1071-8.
2. Gabrielli B, Brooks K, Pavey S. Defective cell cycle checkpoints as targets for anti-cancer therapies. *Frontiers in pharmacology* 2012;3:9.
3. Schlegel R, Pardee AB. Caffeine-induced uncoupling of mitosis from the completion of DNA replication in mammalian cells. *Science* 1986;232(4755):1264-6.
4. Bunch RT, Eastman A. Enhancement of cisplatin-induced cytotoxicity by 7-hydroxystaurosporine (UCN-01), a new G2-checkpoint inhibitor. *Clinical cancer research : an official journal of the American Association for Cancer Research* 1996;2(5):791-7.
5. Zuazua-Villar P, Rodriguez R, Gagou ME, Eyers PA, Meuth M. DNA replication stress in CHK1-depleted tumour cells triggers premature (S-phase) mitosis through inappropriate activation of Aurora kinase B. *Cell death & disease* 2014;5:e1253.
6. Montano R, Chung I, Garner KM, Parry D, Eastman A. Preclinical development of the novel Chk1 inhibitor SCH900776 in combination with DNA-damaging agents and antimetabolites. *Molecular cancer therapeutics* 2012;11(2):427-38.
7. Parsels LA, Morgan MA, Tanska DM, Parsels JD, Palmer BD, Booth RJ, et al. Gemcitabine sensitization by checkpoint kinase 1 inhibition correlates with inhibition of a Rad51 DNA damage response in pancreatic cancer cells. *Molecular cancer therapeutics* 2009;8(1):45-54.
8. Sorensen CS, Syljuasen RG. Safeguarding genome integrity: the checkpoint kinases ATR, CHK1 and WEE1 restrain CDK activity during normal DNA replication. *Nucleic acids research* 2012;40(2):477-86.
9. Ma CX, Janetka JW, Piwnica-Worms H. Death by releasing the breaks: CHK1 inhibitors as cancer therapeutics. *Trends in molecular medicine* 2011;17(2):88-96.
10. Morgan MA, Parsels LA, Maybaum J, Lawrence TS. Improving the efficacy of chemoradiation with targeted agents. *Cancer discovery* 2014;4(3):280-91.
11. Li D, Xie K, Wolff R, Abbruzzese JL. Pancreatic cancer. *Lancet* 2004;363(9414):1049-57.
12. Olive KP, Jacobetz MA, Davidson CJ, Gopinathan A, McIntyre D, Honess D, et al. Inhibition of Hedgehog signaling enhances delivery of chemotherapy in a mouse model of pancreatic cancer. *Science* 2009;324(5933):1457-61.
13. Parsels LA, Qian Y, Tanska DM, Gross M, Zhao L, Hassan MC, et al. Assessment of chk1 phosphorylation as a pharmacodynamic biomarker of chk1 inhibition. *Clinical cancer research : an official journal of the American Association for Cancer Research* 2011;17(11):3706-15.
14. Del Nagro CJ, Choi J, Xiao Y, Rangell L, Mohan S, Pandita A, et al. Chk1 inhibition in p53-deficient cell lines drives rapid chromosome fragmentation followed by caspase-independent cell death. *Cell cycle* 2014;13(2):303-14.
15. Sakaue-Sawano A, Kurokawa H, Morimura T, Hanyu A, Hama H, Osawa H, et al. Visualizing spatiotemporal dynamics of multicellular cell-cycle progression. *Cell* 2008;132(3):487-98.
16. On KF, Chen Y, Ma HT, Chow JP, Poon RY. Determinants of mitotic catastrophe on abrogation of the G2 DNA damage checkpoint by UCN-01. *Molecular cancer therapeutics* 2011;10(5):784-94.

17. Zeman MK, Cimprich KA. Causes and consequences of replication stress. *Nature cell biology* 2014;16(1):2-9.
18. Ashley AK, Shrivastav M, Nie J, Amerin C, Troksa K, Glanzer JG, et al. DNA-PK phosphorylation of RPA32 Ser4/Ser8 regulates replication stress checkpoint activation, fork restart, homologous recombination and mitotic catastrophe. *DNA repair* 2014;21:131-9.
19. Polo SE, Jackson SP. Dynamics of DNA damage response proteins at DNA breaks: a focus on protein modifications. *Genes & development* 2011;25(5):409-33.
20. Shechter D, Costanzo V, Gautier J. ATR and ATM regulate the timing of DNA replication origin firing. *Nature cell biology* 2004;6(7):648-55.
21. Mankouri HW, Huttner D, Hickson ID. How unfinished business from S-phase affects mitosis and beyond. *The EMBO journal* 2013;32(20):2661-71.
22. Zachos G, Black EJ, Walker M, Scott MT, Vagnarelli P, Earnshaw WC, et al. Chk1 is required for spindle checkpoint function. *Developmental cell* 2007;12(2):247-60.
23. Aarts M, Sharpe R, Garcia-Murillas I, Gevensleben H, Hurd MS, Shumway SD, et al. Forced mitotic entry of S-phase cells as a therapeutic strategy induced by inhibition of WEE1. *Cancer discovery* 2012;2(6):524-39.
24. Beeharry N, Rattner JB, Caviston JP, Yen T. Centromere fragmentation is a common mitotic defect of S and G2 checkpoint override. *Cell cycle* 2013;12(10):1588-97.
25. Stevens JB, Abdallah BY, Liu G, Ye CJ, Horne SD, Wang G, et al. Diverse system stresses: common mechanisms of chromosome fragmentation. *Cell death & disease* 2011;2:e178.
26. Stevens JB, Abdallah BY, Regan SM, Liu G, Bremer SW, Ye CJ, et al. Comparison of mitotic cell death by chromosome fragmentation to premature chromosome condensation. *Molecular cytogenetics* 2010;3:20.
27. Morgan MA, Parsels LA, Parsels JD, Mesiwala AK, Maybaum J, Lawrence TS. Role of checkpoint kinase 1 in preventing premature mitosis in response to gemcitabine. *Cancer research* 2005;65(15):6835-42.
28. McNeely S, Conti C, Sheikh T, Patel H, Zabludoff S, Pommier Y, et al. Chk1 inhibition after replicative stress activates a double strand break response mediated by ATM and DNA-dependent protein kinase. *Cell cycle* 2010;9(5):995-1004.
29. Matthews DJ, Yakes FM, Chen J, Tadano M, Bornheim L, Clary DO, et al. Pharmacological abrogation of S-phase checkpoint enhances the anti-tumor activity of gemcitabine in vivo. *Cell cycle* 2007;6(1):104-10.
30. Toledo LI, Altmeyer M, Rask MB, Lukas C, Larsen DH, Povlsen LK, et al. ATR prohibits replication catastrophe by preventing global exhaustion of RPA. *Cell* 2013;155(5):1088-103.
31. Kubara PM, Kerneis-Golsteyn S, Studeny A, Lanser BB, Meijer L, Golsteyn RM. Human cells enter mitosis with damaged DNA after treatment with pharmacological concentrations of genotoxic agents. *The Biochemical journal* 2012;446(3):373-81.
32. Syljuasen RG, Jensen S, Bartek J, Lukas J. Adaptation to the ionizing radiation-induced G2 checkpoint occurs in human cells and depends on checkpoint kinase 1 and Polo-like kinase 1 kinases. *Cancer research* 2006;66(21):10253-7.
33. Montano R, Thompson R, Chung I, Hou H, Khan N, Eastman A. Sensitization of human cancer cells to gemcitabine by the Chk1 inhibitor MK-8776: cell cycle perturbation and impact of administration schedule in vitro and in vivo. *BMC cancer* 2013;13:604.

34. Daud AI, Ashworth MT, Strosberg J, Goldman JW, Mendelson D, Springett G, et al. Phase I Dose-Escalation Trial of Checkpoint Kinase 1 Inhibitor MK-8776 As Monotherapy and in Combination With Gemcitabine in Patients With Advanced Solid Tumors. *Journal of clinical oncology : official journal of the American Society of Clinical Oncology* 2015.
35. Sausville E, Lorusso P, Carducci M, Carter J, Quinn MF, Malburg L, et al. Phase I dose-escalation study of AZD7762, a checkpoint kinase inhibitor, in combination with gemcitabine in US patients with advanced solid tumors. *Cancer chemotherapy and pharmacology* 2014;73(3):539-49.
36. Andre N, Carre M, Pasquier E. Metronomics: towards personalized chemotherapy? *Nature reviews Clinical oncology* 2014;11(7):413-31.
37. Sturgeon CM, Roberge M. G2 checkpoint kinase inhibitors exert their radiosensitizing effects prior to the G2/M transition. *Cell cycle* 2007;6(5):572-5.

FIGURE LEGENDS

Figure 1. Sub-GI₅₀ concentrations of gemcitabine and CHK1i yield effective synergy.

(A) Chemical structure of CHK1 inhibitor S1181.

(B) Cytotoxicity assay. MIA PaCa-2 cells were treated with gemcitabine (x-axis) and S1181 (y-axis) in an 8 X 8 concentration checkerboard format for 72 hours. Cell viability was determined by measuring the total protein content using the sulforhodamine B assays. The experimental data (left, values are percentage growth inhibition compared to control) was analyzed independently with the three synergy models (Bliss, Loewe, Highest Single Agent). The predicted inhibition data by these models (middle) was subtracted from the experimental data (left), yielding a final difference value for each combination (right). The greater a difference value was, the more synergistic that particular combination was. Concentrations that yielded effective synergy (as defined in the text) are boxed in white in Data-Prediction panel. Data are represented as mean \pm SD, n=4.

(C) Immunoblotting for MIA PaCa-2 and Panc-1 cells treated for 24 hours as indicated. Ponceau S was used as loading control. Asterisk indicates that Panc-1 lysates for the CHK1 S296 blot were from a 72-hour treatment.

(D) Immunofluorescence for ATM S1981. MIA PaCa-2 cells were treated with either vehicle or 10nM gemcitabine+1uM S1181 for 24 hours. Scale bar, 20um.

(E) Clonogenic assays. Cells were treated for 72 hours, re-plated in fresh medium and left to grow for 7 days. Data are represented as mean \pm SEM, n=3. *p \leq 0.05, **p \leq 0.01, ***p \leq 0.001, ****p \leq 0.0001.

Note to all figures: Where applicable, treatments were done at synergistic concentrations, i.e. HT-29 (1uM S1181/30nM gemcitabine), K8484 (1uM

S1181/10nM gemcitabine), MIA PaCa-2 (1uM S1181/10nM gemcitabine), Panc-1 (3uM S1181/30nM gemcitabine).

Figure 2. G2/M checkpoint abrogation does not portend effective synergy.

(A) Quantification of immunoblots for Panc-1 cells treated as indicated. Data are normalized to control and are represented as mean \pm SEM, n=3. **p \leq 0.01, ***p \leq 0.001, ****p \leq 0.0001.

(B) Quantification of DNA content of G1 and mitotic MIA PaCa-2 cells treated as indicated. Data are represented as mean \pm SEM. G1 cells (n=250) and pHH3+ cells (n=30-50) were scored per sample. N denotes genetic content as quantified by DAPI staining.

(C) Immunoblotting for Panc-1 cells treated as indicated.

(D) Immunoblotting for K8484 cells treated as indicated.

(E) 2D scatter diagrams for HT-29 cells treated as indicated. Propidium iodide was used as the surrogate for DNA content. Percentage of cells in the two upper quadrants is shown.

(A-E) Treatments were done for 24 hours. Where applicable, synergistic concentrations were used (refer to Figure 1 legend) and were indicated in square brackets in Fig. B-D.

Figure 3. S/G2 progression is a distinct predictor of cell fate.

(A) Cell cycle profiles for MIA PaCa-2 cells treated for 24 hours as indicated. Synergistic concentrations were used, i.e. 10nM gemcitabine, 1uM S1181, 20nM CHIR-124. For quantification of S-phase population with S1181, see Supplementary Table S2.

(B) S/G2 duration in MIA PaCa-2 Fucci cells treated as indicated and imaged by time-lapse microscopy as described in Supplementary Materials and Methods. S/G2

duration was defined as the interval between the time geminin (green fluorescence) was detected to the time of its disappearance. A total of 2191 cells were pooled from two biological replicates for analysis. Data are represented as mean \pm SEM.

**** $p \leq 0.0001$.

(C) Time-lapse sequences illustrating deleterious fates exhibited by MIA PaCa-2 Fucci cells upon 10nM gemcitabine+1uM S1181 treatment. Scale bar, 50um.

(D) Fate profiles of 115 individual MIA PaCa-2 Fucci cells from the point of 10nM gemcitabine+1uM S1181 treatment to the end of the first observed mitosis (if occurred). Solid bar denotes the duration of the specified phase of each 1st-generation cell and is ranked according to S/G2 duration (green bar). Dotted bar denotes the outcome of the observed mitosis without further temporal reference. Truncated bar denotes cell elimination at that phase.

(E) Fates of 150 daughter MIA PaCa-2 Fucci cells treated with 10nM gemcitabine+1uM S1181 (blue = successful cytokinesis, red = cytokinesis failure, black = death/senescence/interphase arrest) correlated with their maternal S/G2 and mitotic durations. Data are represented as mean \pm SEM. The slope and p-value obtained from a linear regression analysis are shown.

(F) Cross-generation S/G2 duration in MIA PaCa-2 Fucci cells treated with 10nM gemcitabine+1uM S1181. Cells that were initially at G1 (1st generation) that subsequently produced at least one dividing daughter (2nd generation) were tracked for their S/G2 durations. Blue marks cells with successful cytokinesis, red marks cells that failed to divide. Data are represented as mean \pm SEM. A paired two-tailed t-test was used for significance, **** $p \leq 0.0001$.

(D-F) Data were pooled from three biological replicates for analysis.

Figure 4. Deregulated DNA replication causes synergistic growth inhibition.

(A) EdU incorporation. Double thymidine-synchronized MIA PaCa-2 cells were released into indicated treatment conditions labelled with 10uM EdU, fixed at specified intervals and assayed for EdU signal (Click-it reaction). Quantitative microscopy was performed to determine the total and maximal EdU intensities per nucleus for each of >3500 individual cells/sample. Percentages of positive cells (blue) are shown.

(B) Immunofluorescence in cells treated for 24 hours as indicated. Quantitative microscopy was performed to determine the total fluorescence intensities per nucleus. Respectively, blue, yellow and red mark individual cells that were positive for γ H2AX, for RPA32 S4/8 and for both markers. Percentages of double-positive cells are shown.

(C) Cell cycle profiles of MIA PaCa-2 cells treated for 12 hours as indicated. Profile for gemcitabine+S1181 sample (gray) serves as background reference.

(D) Immunofluorescence in Panc-1 cells treated for 24 hours as indicated. Quantitative microscopy was performed. Respective percentages of γ H2AX only (blue), RPA32 S4/8 only (yellow) and γ H2AX+RPA32 S4/8 positive (red) cells are shown.

(E) Cell proliferation in K8484 cells treated as indicated. Three random fields of view per sample were imaged by time-lapse microscopy at every 3 hours. Data are represented as mean \pm SEM, n=3. Area under the curve was used as the surrogate for growth over time. A two-tailed t-test was used for significance between GEM+S1181 and GEM+S1181+Roscovitine or GEM+S1181+Cdc7i from three independent experiments. * $p \leq 0.05$.

(A-E) Treatments were done at synergistic concentrations (refer to Figure 1 legend). Roscovitine and Cdc7i were used at 10uM and 1uM, respectively.

Figure 5. Cumulative chromosomal aberrations are due to replication stress.

(A) Mitotic aberrations in MIA PaCa-2 cells treated with gemcitabine+S1181.

Arrowhead denotes lagging chromosomes (top) and anaphase bridge (bottom).

Scale bar, 10um.

(B) Quantification of mitotic aberrations in cells treated for 24 hours as indicated.

>200 mitotic cells per condition on average were scored. Data are represented as mean \pm SEM, n=3-5. * $p \leq 0.05$, ** $p \leq 0.01$, **** $p \leq 0.0001$.

(C) Stacked confocal images of misaligned metaphases of MIA PaCa-2 cells treated with gemcitabine+S1181 and stained as indicated. Scale bar, 10um.

(D) Mitoses of MIA PaCa-2 cells treated with gemcitabine+S1181 and stained as indicated. Scale bar, 5um.

(E) Stacked confocal image of aberrant HT-29 mitotic cell (arrowhead) treated with gemcitabine+S1181. EdU-positive cells were outlined with dotted line. Scale bar, 10um.

(F) Representative metaphase spreads of MIA PaCa-2 cells treated with gemcitabine+S1181 for 24-72 hours. Scale bar, 10um.

(A-F) Treatments were done at synergistic concentrations (refer to Figure 1 legend).

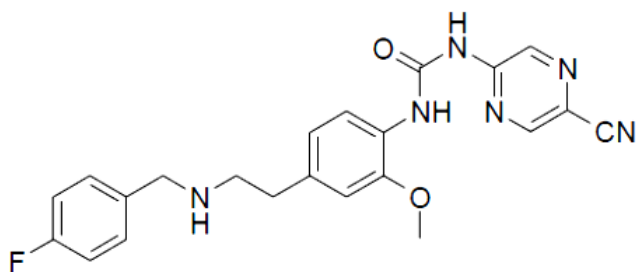
Figure 6. Molecular and cellular responses to treatment are concentration-sensitive.

(A) A generalized model on the modulation of mitotic CDK1 and mitotic states by gemcitabine and CHK1i.

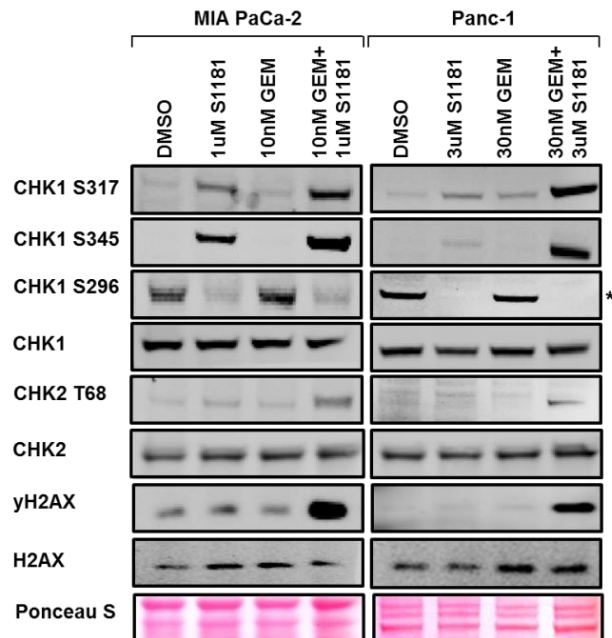
(B) A “foot-in-the-door” model of cell fates upon treatment with synergistic concentrations of gemcitabine and CHK1i.

Figure 1

(A)



(C)

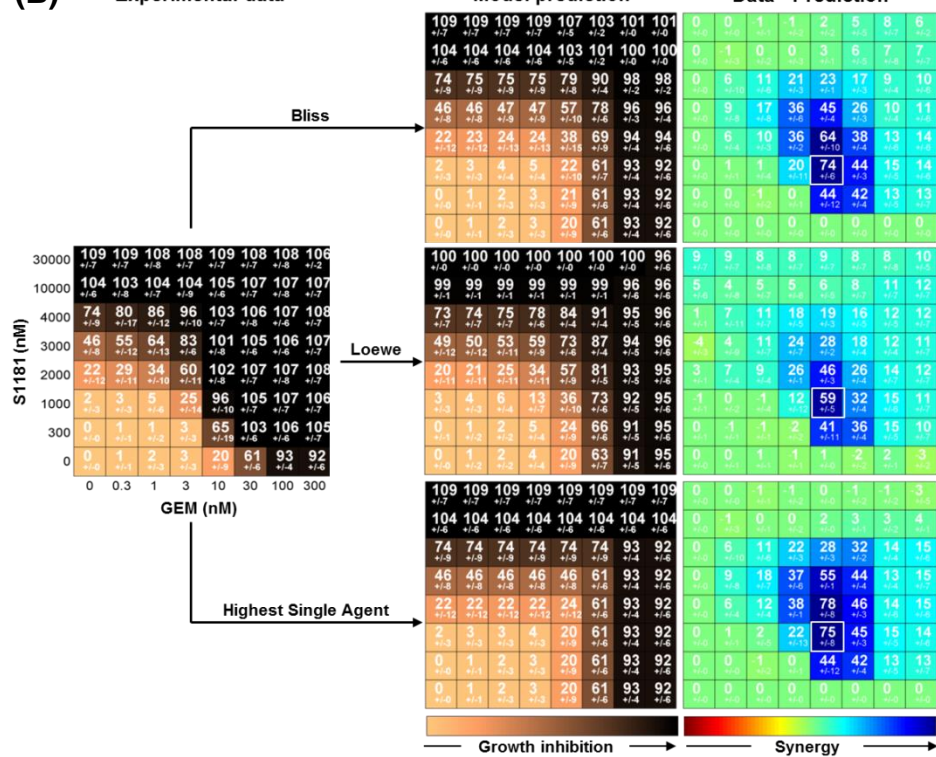


(B)

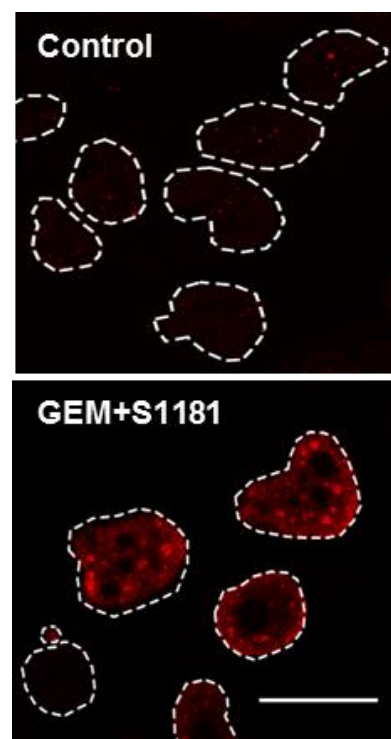
Experimental data

Model prediction

Data - Prediction



(D)



(E)

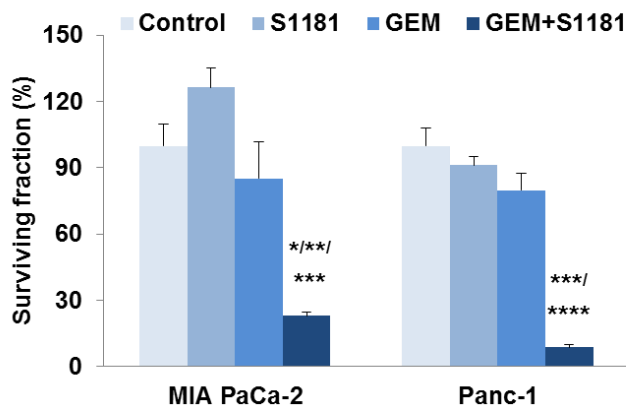
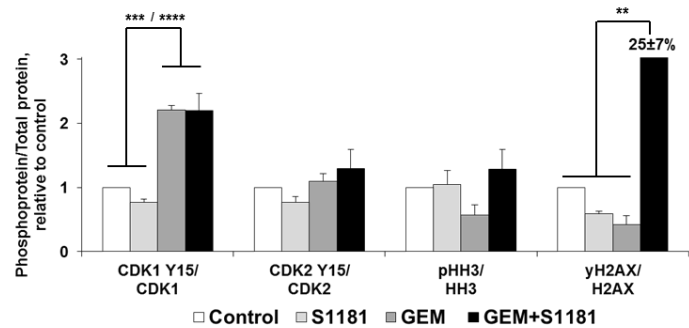
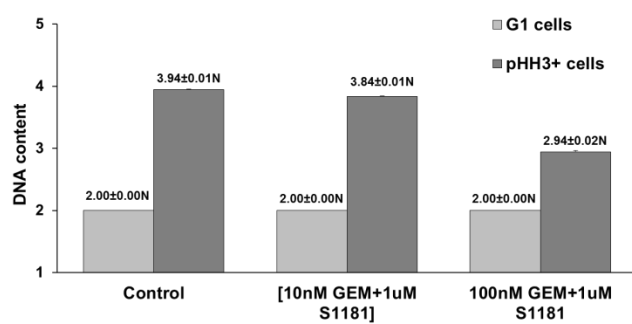


Figure 2

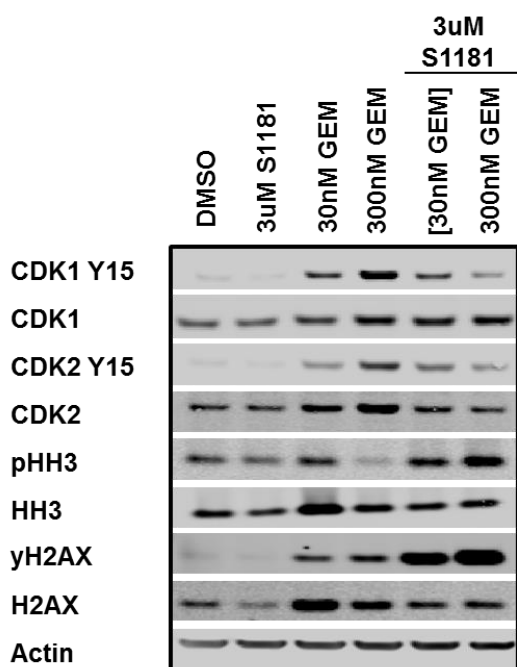
(A)



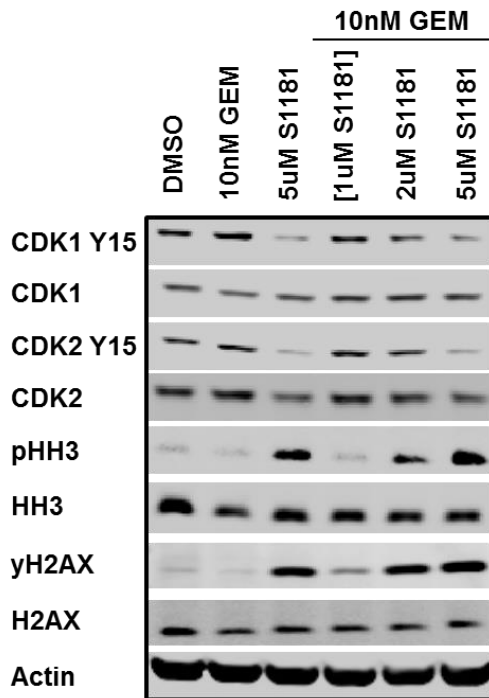
(B)



(C)



(D)



(E)

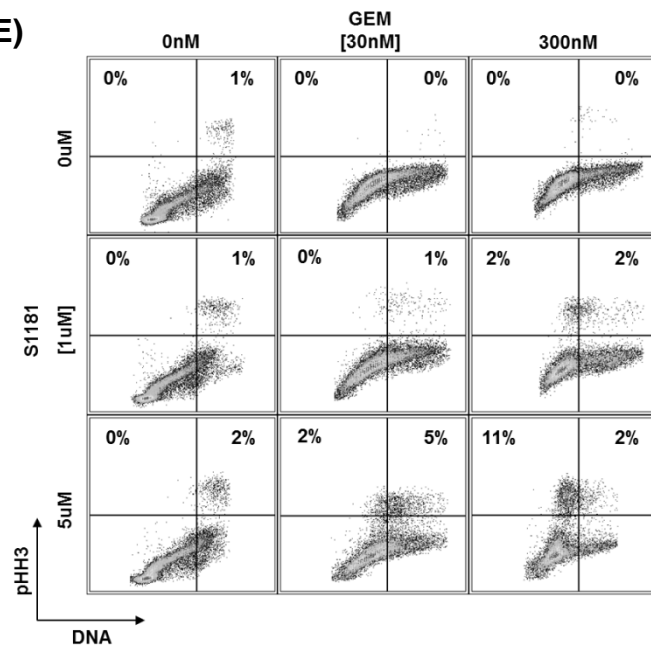


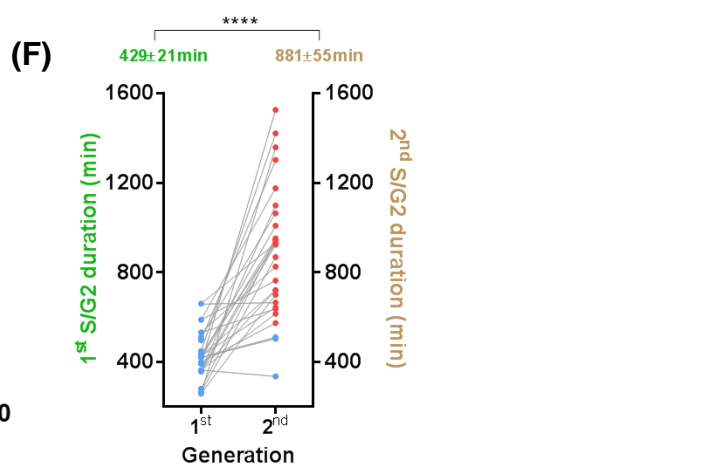
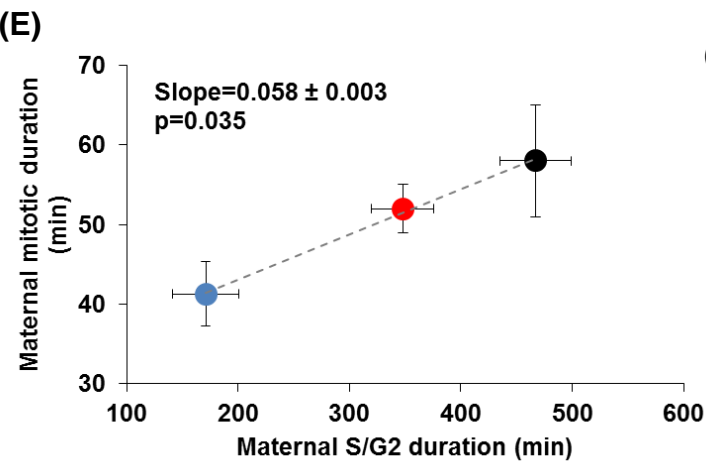
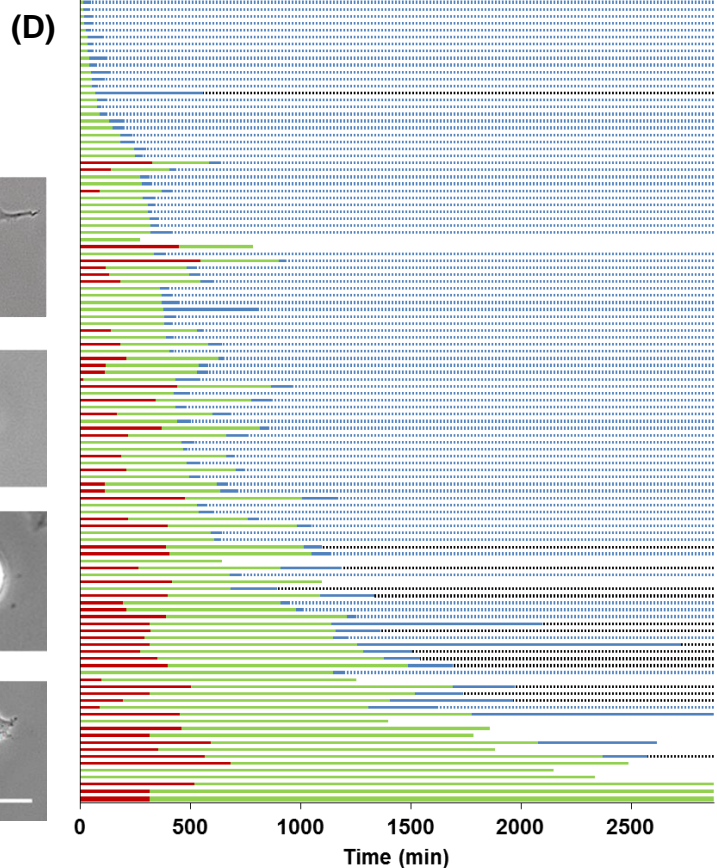
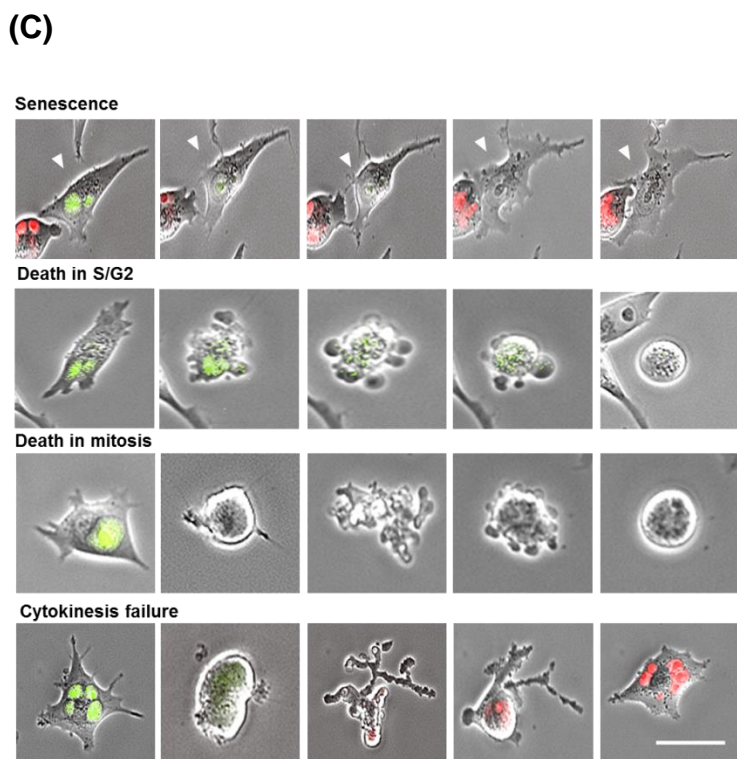
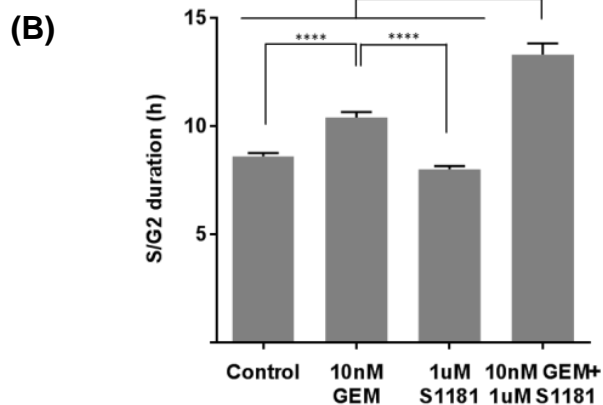
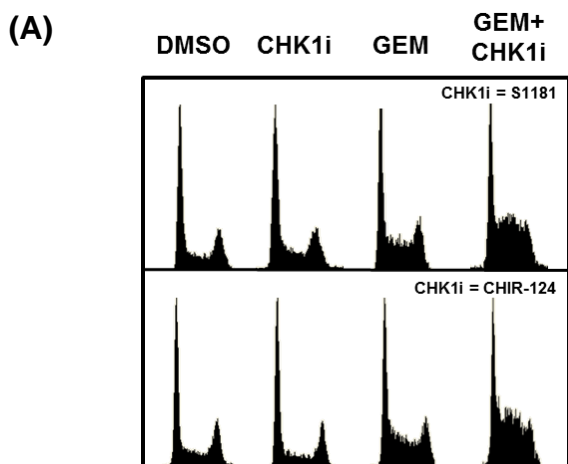
Figure 3

Figure 4

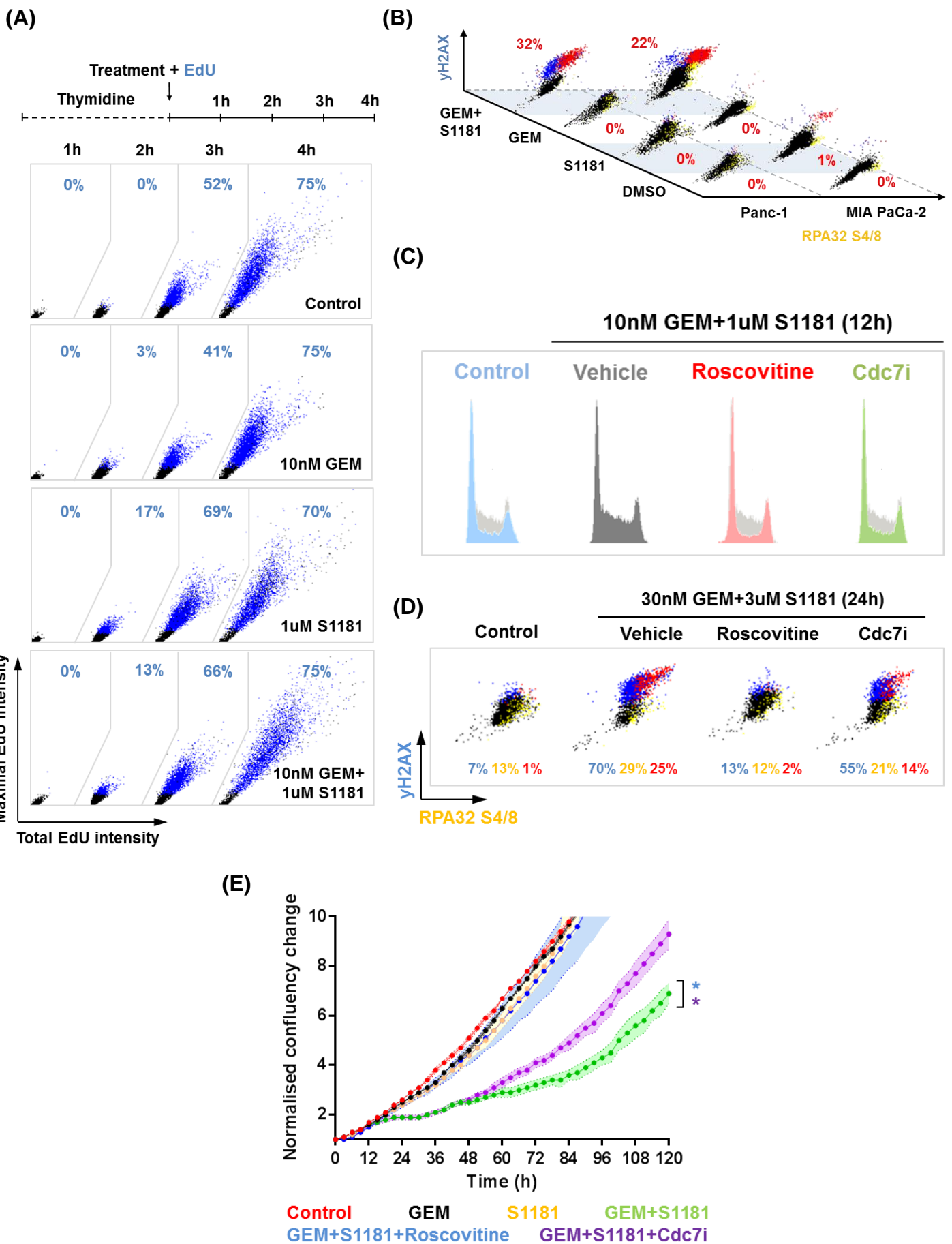


Figure 5

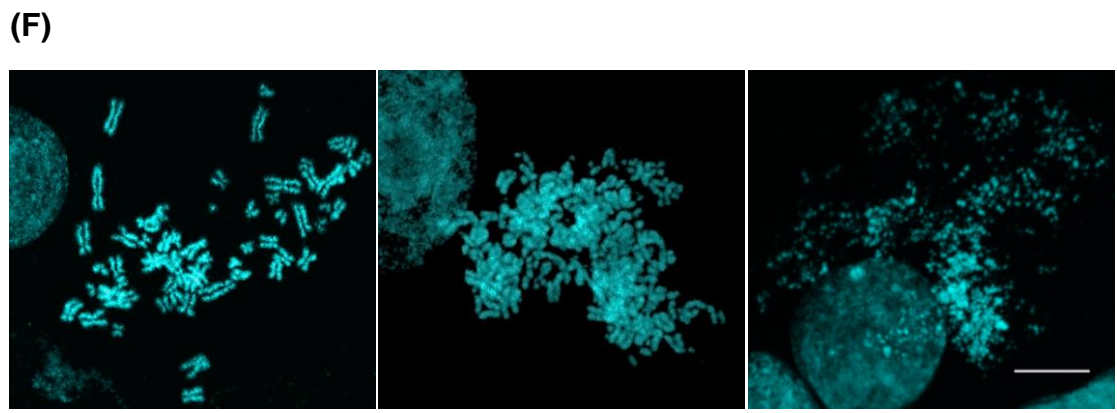
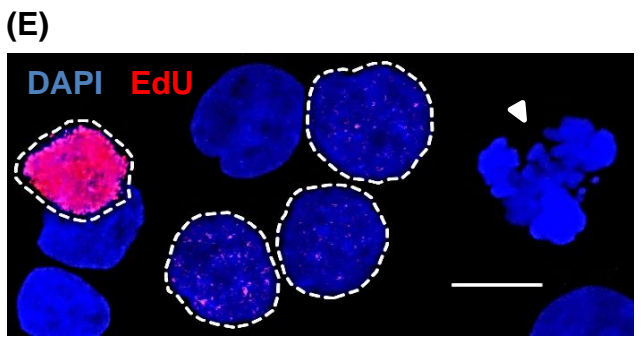
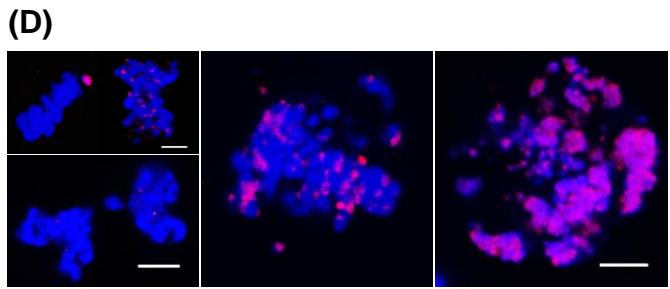
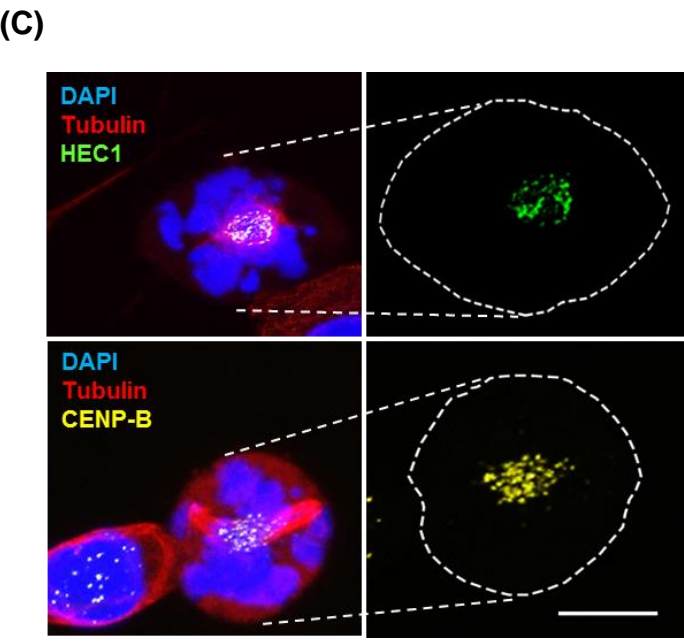
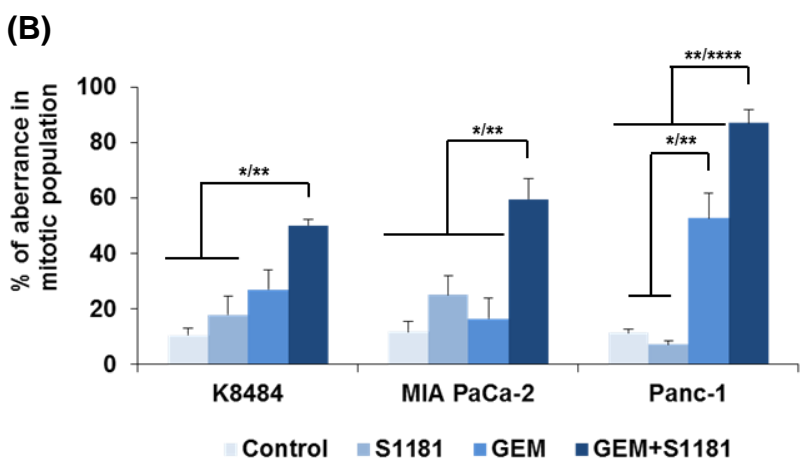
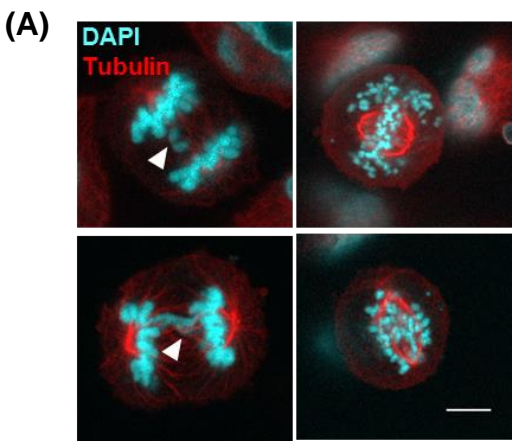
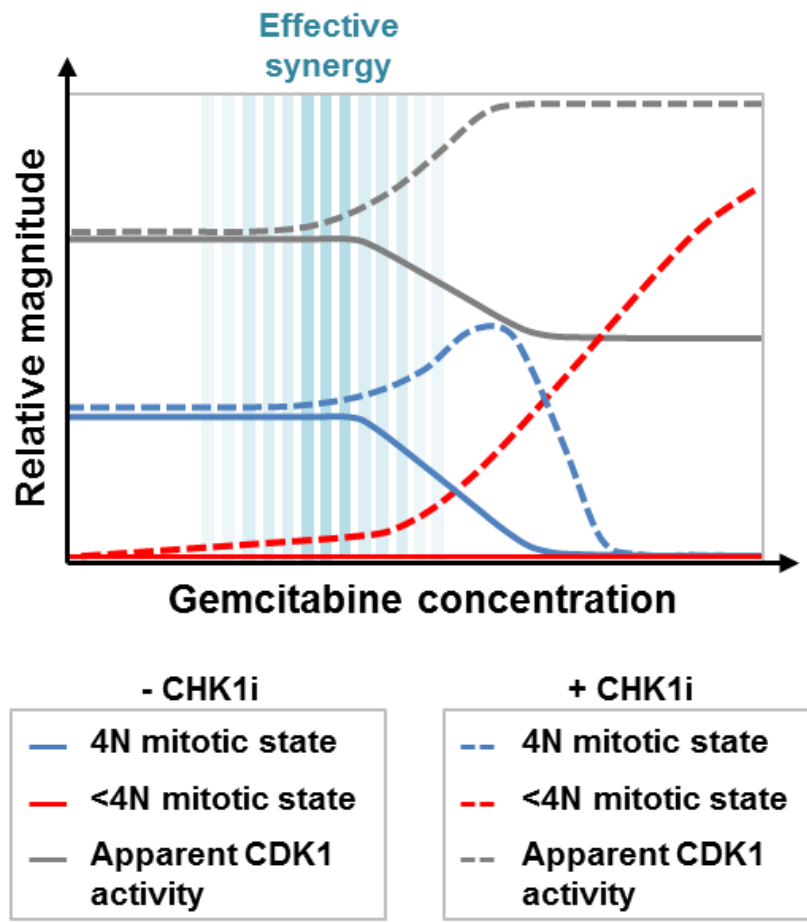


Figure 6

(A)



(B)

